JOURNAL OF MATERIALS SCIENCE 26 (1991) 423–428

Anodic polarization of HgTe, CdTe and $Hg_{0.8}Cd_{0.2}Te$ – oxide formation kinetics and composition

R. D. S. YADAVA, A. V. R. WARRIER
Solid State Physics Laboratory, Lucknow Road, Delhi 110 054, India

A comparative study of the anodic polarization behaviour of HgTe, CdTe and $Hg_{0.8}Cd_{0.2}Te$ at constant current density was undertaken. It is argued that metal dissolution starts first, which renders the semiconductor surface negatively charged and tellurium rich. The process continues until the overpotential across the interface rises sufficiently to dissociate the tellurium at which point tellurium dissolution and oxidation begins. The continuation of this process evidently requires that the metal dissolution follows. This dissolution–precipitation mechanism for oxide nucleation is supported here. It is predicted that the molar ratio of $HgTeO_3$ to $CdTeO_3$ in the anodic oxide on $Hg_{0.8}Cd_{0.2}Te$ should be ~ 1.1. This is in good agreement with the experiments. The overvoltages required to initiate oxidation are shown to decrease when the current density is increased.

1. Introduction

Surface preparation and passivation are important steps in producing high-performance infrared detectors from $Hg_{1-x}Cd_xTe$ crystals. Usually bromine methanol polish and etch are employed for the former and anodic oxidation in KOH solution for the latter. The characteristics of the semiconductor–oxide interface (surface state density, surface recombination velocity and low-frequency noise) depend upon both treatments. Therefore, a detailed understanding of the electrochemical nature of the semiconductor is required. Recently, several publications have appeared dealing with surface stoichiometry, oxide growth mechanism and composition [1–14]. However, there still remains much to be understood.

Lastras–Martinez *et al.* [1] reported that the bromine methanol etch damages the crystal surface by depleting it of cadmium and leaving a tellurium-rich layer up to a depth of ~ 60 nm. A sequence of anodization–dissolution steps was shown to remove this damaged layer, though when continued beyond the damage depth a further cadmium-deficient and tellurium-rich zone is created towards the semiconductor side of the interface [1]. In other reports, Rhiger and Kvaas [2] and Sakashita *et al.* [3] also reported cadmium depletion after a bromine methanol etch, and a cadmium-deficient semiconductor–oxide interface after anodic oxidation. Richter *et al.* [4] and Morgen *et al.* [5], however, reported no significant change in the interface stoichiometry. Sun *et al.* [6], Davis *et al.* [7] and Ahearn *et al.* [8], on the other hand, reported that a mercury-deficient zone of ~ 20 nm is formed at the interface as a result of anodic oxidation. Ahearn *et al.* [8] also report to the contrary that the bromine methanol etch produces a thin mercury-rich surface layer.

Questions relating to the mechanism of oxide nucleation, growth and composition also are not fully answered. Janousek and Carscallen [9] supported the dissolution–precipitation mechanism for nucleation, and metal cation outdiffusion towards the electrolyte and/or hydroxyl anion successive-jump transport towards the interface through the film for the bulk growth process. According to their model, the initial oxidation products at the semiconductor–electrolyte interface are dissolved and diffused away in the solution. Owing to imbalance between dissolution and diffusion rates, the semiconductor surface becomes either electroetched (if the former is smaller than the latter), or the concentration of oxidation products builds up at the interface until it exceeds the solubility limit, and an incipient oxide film is precipitated on the surface. Anodic polarization curves with sweeping voltage [8, 9] exhibit two peaks. Ahearn *et al.* [8] assign the first peak to the stripping of excess mercury at the surface produced by the bromine methanol etch and the second peak to tellurium oxidation accompanied by further dissolution of mercury. Janousek and Carscallen [9], however, assign the first peak to cadmium oxidation and the second peak to tellurium oxidation. Similarly, Strong [10] has also recently concluded that the bulk oxide growth occurs by the hopping of oxygen ions into neighbouring oxygen vacancies towards the oxide–semiconductor interface (or oxygen vacancy outdiffusion towards the oxide–electrolyte interface).

The composition of anodic oxides has also been extensively studied; however, the uncertainty still prevails. No agreement on this issue exists amongst the various authors [2–11]. Recent reports by Seelman–Eggebert *et al.* [12], Stahle *et al.* [13] and Strong *et al.* [14] clarify that earlier confusion

0022–2461/91 $03.00 + .12

was due to changes in composition caused by ion-beam sputtering during elemental analysis. Seelman–Eggebert *et al.* [12] conclude that $HgTeO_3$ and $CdTeO_3$ are the only constituents of the anodic oxide, and the $CdTeO_3$ mole fraction, m, lies in the range $x < m < 1$. For $x = 0.2$ crystals, they inferred $m \simeq 0.55$, and the corresponding Hg/Cd ratio to be 0.82. Stahle *et al.* [13] and Strong *et al.* [14] concluded that the main constituents of anodic oxide are $HgTeO_3$, $CdTeO_3$ and TeO_2. For oxides on $x = 0.22$ crystals, they found Hg/Cd = 1.57, and for $x = 0.202$, Hg/Cd = 2.80.

A comparative study of the anodic polarization behaviour of HgTe, CdTe and $Hg_{0.8}Cd_{0.2}Te$ at constant current densities is presented here. This helps in identifying the dominant electrochemical reaction at the interface during the nucleation stage of oxide formation. By combining the present results with previously published reports of other authors, a coherent picture of oxide formation kinetics may be presented.

2. Experimental procedure

Experiments were carried out on single-crystal wafers of $Hg_{0.8}Cd_{0.2}Te$ prepared by solid state recrystallization in our laboratory [15–17]. The HgTe and CdTe crystals were as-grown without any special annealing treatment. The $Hg_{0.8}Cd_{0.2}Te$ crystals were n-type prepared by annealing in a mercury atmosphere. These crystals had electron densities in the range 1 to 5 $\times 10^{15}$ cm^{-3} at 77 K. Samples of sizes about 4 × 1 × 0.5 mm^3 were epoxied on to saphire discs and their surfaces were prepared by lapping with 1 μm alumina and chemomechanical polishing in 2% bromine methanol solution. Before anodization, the samples were etched for 30 sec in the same solution and rinsed thoroughly with methanol. The copper leads were attached to them with indium solder. The contact and that part of the lead which dipped into the electrolyte were covered with a lacquer. The electrolyte was 0.1 M KOH in 90% ethylene glycol and 10% deionized water. A platinum sheet was used as the cathode and its separation from the semiconductor anode was always kept at 1 cm. The samples were anodized at constant current density over the range 100 to 1000 μA cm^{-2}. The cell voltage–time curves (anodic charging/polarization curves) were recorded with an X–Y recorder.

3. Results and discussion

3.1. Relative behaviour of HgTe, CdTe and $Hg_{0.8}Cd_{0.2}Te$ at 100 μA cm^{-2}

Prior to imposing the external current source, the anodization cell is in equilibrium. Energetically the most favourable redox reaction at the semiconductor–electrolyte interface establishes the equilibrium cell voltage. Based upon some known general facts, we first argue and assume a reaction model which establishes the equilibrium. The moment an electrode–electrolyte system comes into contact, charge transfer reactions at the interface start spontaneously, the electrical double layer builds up and the equilibrium electrode potential is established. The reaction for which the exchange current density is highest governs the electrochemical behaviour of the electrode. The exchange current density depends upon the free-energy change associated with the reaction and the activity of the ions/atoms involved. Of the three elements in question here, cadmium is the most electropositive and tellurium the least [18]. Therefore, cadmium has the highest tendency to ionize as Cd^{2+} ions, followed by mercury. On the other hand, tellurium is fairly electronegative (electronegativity ~ 3.59 [18]), and hence it has high tendency to accept electrons. Therefore, the likely reaction mechanism at the interface seems to be the dissolution of metal atoms in the solution as cations, leaving behind a negatively charged tellurium-rich layer on the semiconductor side. This reaction model is consistent with several experimental findings on surface stoichiometry as mentioned in Section 1.

Thus, we assume that the most favourable process is the metal cation dissolution and deposition as per the redox reaction $M \rightleftharpoons M^{2+} + 2e$. When the current is switched on, electrode polarization occurs and the cell voltage changes due to the following factors: (a) the current flow in the circuit requires the above reaction at the interface to proceed in the forward direction. This is facilitated by inducing a potential difference across the interface (activation polarization); (b) if the rate of metal dissolution is higher than the diffusional out-flux in the solution then the ion concentration at the interface increases causing a further potential difference between the solution and the semiconductor (concentration polarization); (c) ohmic drop across the solution resistance between anode and cathode which remains constant during the anodization at constant current. If we assume the platinum cathode to be non-polarizable (the justification for which is provided later) then the change in cell voltage (overvoltage) with time is solely a record of events at the semiconductor–electrolyte interface with time.

Fig. 1 shows such a record for HgTe, CdTe and $Hg_{0.8}Cd_{0.2}Te$ at 100 μA cm^{-2} constant current density anodization. The inset at the right-hand bottom corner shows the variation of cell voltage for the first few seconds with better resolution. The initial cell voltage rises quickly and passes through a sublinear region in each case. This is followed by another pronounced sublinear region in HgTe and $Hg_{0.8}Cd_{0.2}Te$, but not in CdTe. Then comes a slowly varying region (almost a plateau in HgTe), a superlinear region and finally a perfect linear region corresponding to steady state oxidation in each case. Similar curves were also reported for $Hg_{0.7}Cd_{0.3}Te$ by Janousek and Carscallen [9] although there are a few important differences which will be elaborated below.

The different stages of cell voltage variation indicate different processes at the interface. The moment current flow begins the equilibrium double-layer structure is disturbed, the metal cation dissolution increases and the semiconductor side of the interface, which is already tellurium rich, becomes more negatively charged and tellurium rich. However, due to metal depletion at the interface, further dissolution

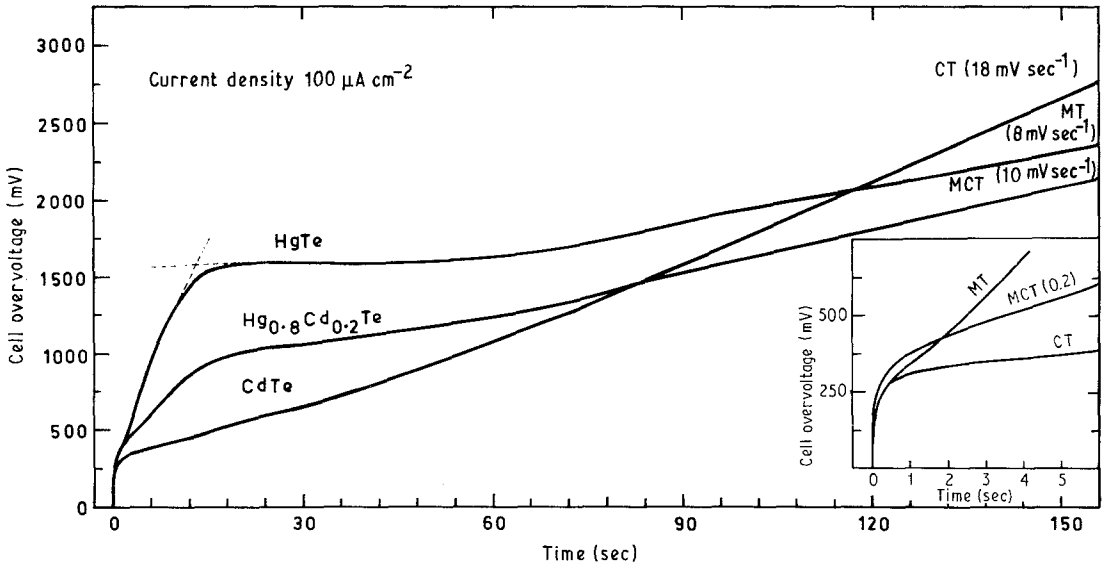

Figure 1 Anodic polarization curves of HgTe, $Hg_{0.8}Cd_{0.2}Te$ and CdTe at 100 μA cm^{-2}; the compounds are also abbreviated as MT, MCT and CT, respectively.

becomes increasingly difficult and to keep pace with the charge transfer rate the activation overvoltage, η_a rises. The imbalance between the charge exchange at the interface and ion transport rate in the solution also causes the concentration overvoltage, η_c, to increase. Thus the first shoulder in each case is identified as the metal dissolution which causes both η_a and η_c to increase, producing an increasing electric field at the interface. Under this field the negatively charged tellurium layer experiences increasing force which tends to dissociate it from the semiconductor matrix. However, the field required to dissociate tellurium depends upon two factors, the degree of ionicity of the bond and the stoichiometric deviation which the lattice can withstand. It is known that the degree of ionicity in the CdTe bond is 0.67 [19] and is higher than that in HgTe, 0.50 [20]. In addition, the stability field of CdTe [21] is quite narrow and relatively symmetric around the perfect stoichiometry, whereas HgTe [22] possesses a wider stability field lying almost entirely on the tellurium-rich side. Therefore, tellurium dissociation from CdTe is much easier and may occur at a much lower electric field than from HgTe. The beginning of the second shoulder is identified as the onset of tellurium detachment in HgTe and $Hg_{0.8}Cd_{0.2}Te$. Its absence in CdTe is because of the above-mentioned differences from the other two compounds. As the cadmium dissolution proceeds and the tellurium-rich layer is formed, the interface becomes highly unstable because no high stoichiometric deviation is allowed. Further cadmium dissolution will not proceed until the excess tellurium is cleared. Thus cadmium and tellurium dissolution and oxidation in the case of CdTe closely accompany each other, and different shoulders are not resolved. On the contrary, HgTe and $Hg_{0.8}Cd_{0.2}Te$ can stand a large stoichiometric deviation towards the tellurium-rich side before tellurium dissolution begins and the large overvoltages are required.

The relatively flat region which follows the second shoulder indicates that this dissolution process is accompanied by an electron-donating reaction. This is, probably the energetically most favourable tellurium oxidation [21]

$$Te + 6OH^- \rightarrow TeO_3^{2-} + 3H_2O + 4e$$

As tellurium dissolution and oxidation proceeds, the surface becomes relatively clear of excess tellurium and the metal dissolution begins to compete. This results in the electroetching of the semiconductor surface and is the dissolution phase of the oxide nucleation mechanism [9]. When the concentration of the metal ions and tellurite ions increases beyond the solubility product at the interface, oxide nucleation at the semiconductor surface begins and marks the onset of the superlinear region. As more and more surface area is covered with the incipient oxide film the cell voltage rises, and when the surface is fully covered, oxide thickening starts, marking the beginning of the linear region.

3.2. Chemical composition of the oxide

The shoulder voltages (taken as the crossing point of the two tangents drawn on either side of the shoulder) are, in fact, critical overvoltages, η_{cr}, required for a particular electrode reaction to occur. They are analogous to activation energies involved in a thermally activated reaction, reaction rate $\propto \exp(-E_a/kT)$ where E_a is the activation energy. Similarly, any other overvoltage, η, is analogous to kT. Therefore, the rate of the reaction at overvoltage η will be proportional to $\exp(-\eta_{cr}/\eta)$. The rate of reaction is also proportional to the activity of the reactants. From the above identification, the highest shoulder voltages observed are the critical overvoltages required to initiate the oxidation of the electrodes. Further, in view of the experimental findings of Seelman–Eggebert *et al.* [12], if we assume that the oxidation products are $CdTeO_3$ and $HgTeO_3$ only, the rate of formation, R, of these anodic products at the shoulder voltages in $Hg_{1-x}Cd_xTe$ will be

$$R_{CdTeO_3} \propto x \exp\left(-\frac{\eta_{CdTe}}{\eta_{Hg_{1-x}Cd_xTe}}\right)$$

and

$$R_{HgTeO_3} \propto (1-x)\exp\left(-\frac{\eta_{HgTe}}{\eta_{Hg_{1-x}Cd_xTe}}\right)$$

It is reasonable to assume that the chemical composition of the anodic film contains these products in the same ratio in which they are formed. Therefore, the molar ratio of $HgTeO_3$ to $CdTeO_3$ in the oxide is given by

$$\text{Hg/Cd} = \frac{1-x}{x}\exp\left(-\frac{\eta_{HgTe} - \eta_{CdTe}}{\eta_{Hg_{1-x}Cd_xTe}}\right)$$

It can be seen from Fig. 1 that η_{cr} for HgTe, CdTe and $Hg_{0.8}Cd_{0.2}Te$ are 1525, 263 and 970 mV, respectively. The molar ratio Hg/Cd for $x = 0.2$ is therefore 1.09. This gives a $CdTeO_3$ mole fraction $m \simeq 0.48$. Compare this value with Seelman–Eggebert *et al.*'s value $m \simeq 0.55$; the agreement is fairly good. Thus the present results provide an explanation for the fact that the molar ratio of CdTe and HgTe oxidation products in the anodic film is dramatically different from their ratio in the alloy.

3.3. Variation of anodic polarization of $Hg_{0.8}Cd_{0.2}Te$ with current density

Fig. 2 shows the variation of cell overvoltage with time over a range of current densities. The similarities and

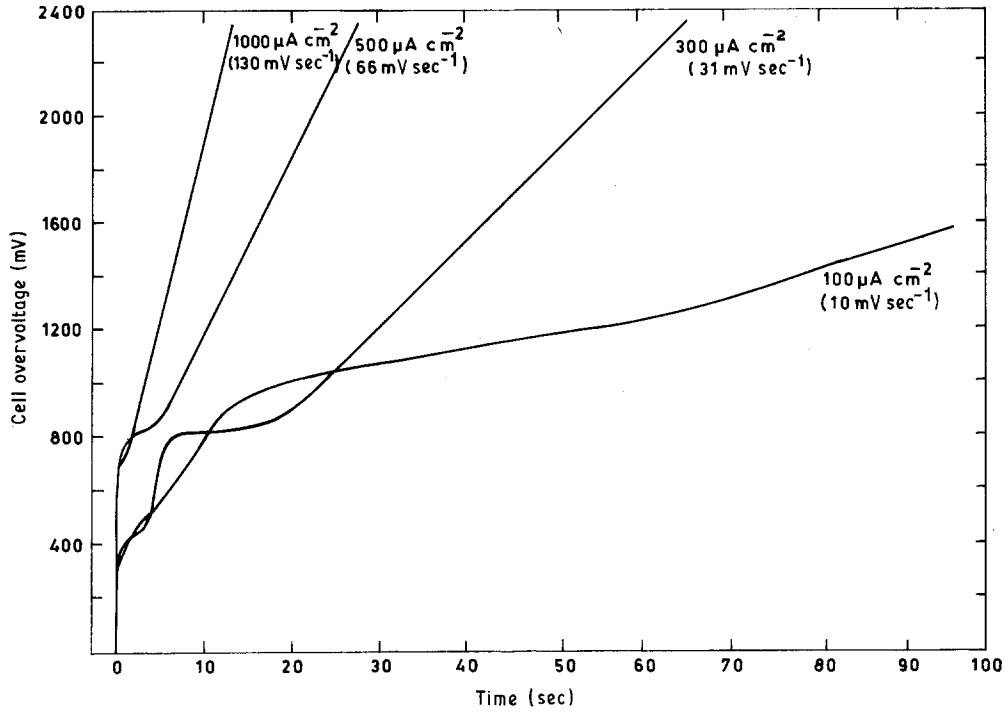

Figure 2 Anodic polarization curves of $Hg_{0.8}Cd_{0.2}Te$ for different current densities.

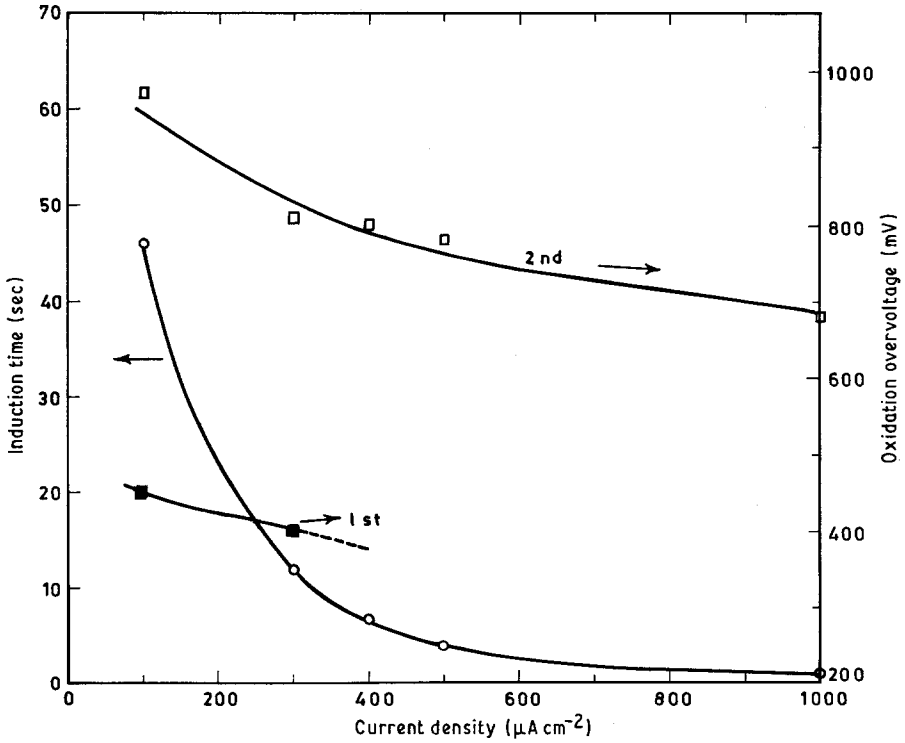

Figure 3 Induction time, and first and second shoulder voltages as a function of anodization current density.

differences of these curves with those reported by Janousek and Carscallen [9] is noteworthy. The length of both plateaus (induction times) decreases with increase in current density. This trend is similar to that given by Janousek and Carscallen [9], and is shown in Fig. 3 for the second plateau. However, both the shoulder voltages decrease with increasing current density, in sharp contrast to that in [9] where it is reported to increase, see Fig. 3. The reduction in shoulder voltages with current density can be qualitatively understood in terms of the latter's effect on the structure of electrical double layer. At high current density the dissolving species at the interface find it difficult to cope with the demand for higher dissolution rate; therefore, the entire Guy–Chapman layer and hence the Helmholtz outer plane is attracted closer to the semiconductor. This process will produce a high electric field at the interface at low overvoltages and keeps the dissolution going. No plausible explanation can be offered for the observed differences between the present results and those given in [9]; however, the reason seems to lie in the difference in composition. For alloys with higher x-values the exchange current density at equilibrium is quite high (because of the higher cadmium content); therefore the dependence of current on activation polarization (Tafel relationship) and concentration polarization [22] probably holds over a large range of current densities; therefore, the overvoltages increase with current density.

Another aspect worth noting is the rate of cell voltage change in the linear region (bulk oxide growth region). With increasing current density it increases almost linearly. However, above about 300 $\mu m\,cm^{-2}$ a small superlinearity arises. This may be due to the following reason: at high current densities the diffusional flux of the anodic products reaches their limiting values, therefore, to cope with the charge transfer rate from the semiconductor to the solution, the precipitation rate increases by a factor more than the increase in current density. The proportionate variation of the oxide growth rate with current density also indicates that the entire overvoltage drops across the semiconductor–oxide–electrolyte region. In other words, the semiconductor electrodes are almost completely polarizable and the platinum cathode is non-polarizable.

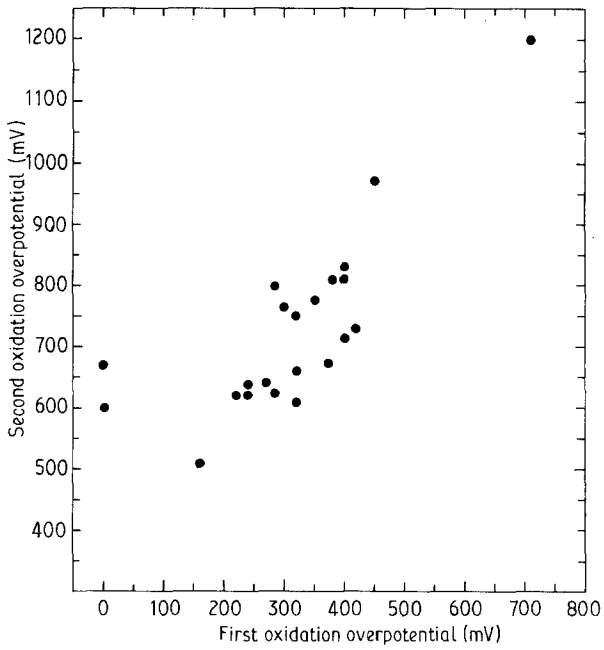

Figure 4 Relationship between the first and second oxidation overvoltages.

3.4. Relationship between first and second overvoltages

No definite relationship could be established between the first and the second overvoltages. However, in

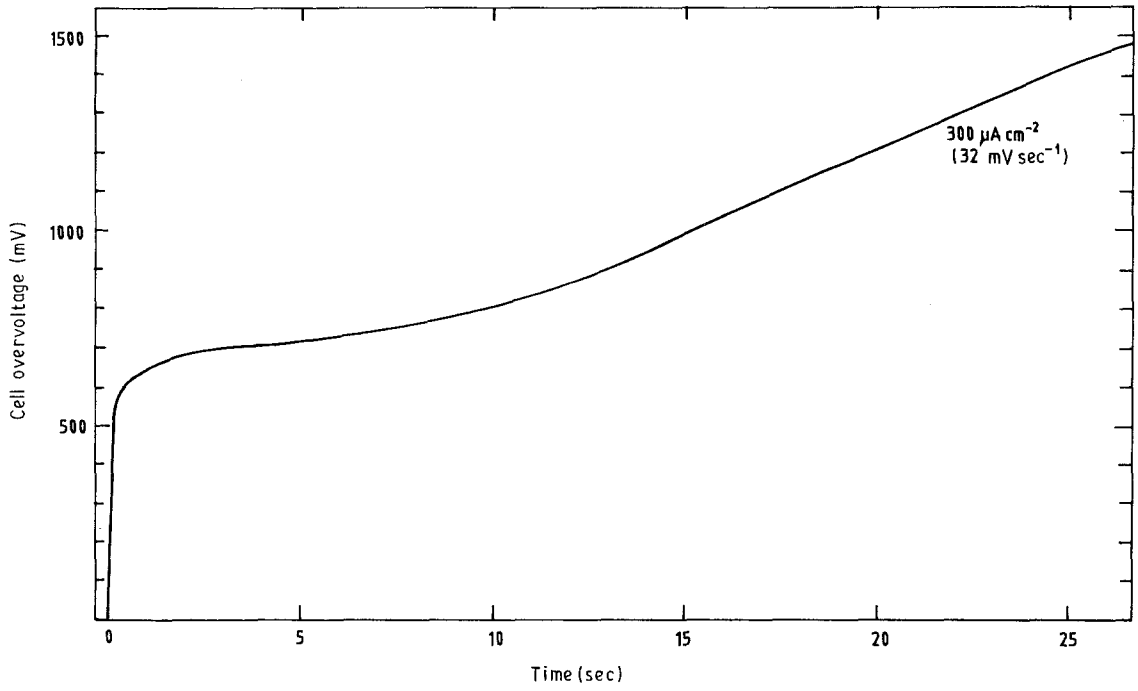

Figure 5 Anodic polarization curve of $Hg_{0.8}Cd_{0.2}Te$ at 300 $\mu A\,cm^{-2}$ after the initial oxide grown at the same current density was stripped.

general the second was lower for a lower first overvoltage. Even for the same anodization conditions, the two voltages showed considerable fluctuation when examined for a large number of samples. Fig. 4 represents the scattered points over a large range for a number of samples anodized over the current density range 20 to 1000 $\mu A\,cm^{-2}$. This is apparently due to the non-reproducibility of the surface condition prior to anodization, because of the random orientation of the crystals and the bromine methanol etch. The former will result in varying kind and density of surface defects from sample to sample and the latter in uncertain stoichiometrically damaged layer [1, 8]. This will markedly influence the initial stages of oxidation. It was noticed in a few cases that after the anodic oxide was removed in very dilute HF solution (about 0.2%) and further anodized, the first shoulder did not appear. One such curve is shown in Fig. 5. This supports the contention that the first shoulder corresponds to the metal dissolution, because the initial oxidation will produce a metal deficient (preferably cadmium deficient because of higher exchange current density) interface having reducing concentration gradient towards the bulk semiconductor. This metal deficiency zone may increase and finally stabilize during bulk oxide growth. After dissolving the oxide this zone is already present on the surface, so during the second anodization the overvoltage rises directly to dissolve and oxidize tellurium.

4. Conclusion

The two peaks appearing in the I–V characteristics of the anodization cell have been correlated to the two shoulder voltages appearing in the overvoltage–time curves under constant current density. The first peak and shoulder voltage correspond to the metal cation dissolution and the second to tellurium dissolution and oxidation. In $Hg_{1-x}Cd_xTe$ alloys, the dissolution rate of cadmium is expected to be greater on the grounds of the low activation potential needed; however, it should be properly weighted by its activity in the alloys. In low x alloys the dissolution rate of both mercury and cadmium may be comparable. The imbalance of these two rates will determine the stoichiometric deviation of the semiconductor oxide interfaces. We favour the dissolution–precipitation model for oxide nucleation. We have shown that the oxide composition could be remarkably different from the molar ratio of the components in the alloy, and a relationship for the entire alloy composition range is predicted. The prediction from this relationship agrees with the available experimental data. It is also shown that the semiconductor electrodes are completely polarizable and the oxidation overvoltages decrease with increasing current density.

Acknowledgements

We thank Drs W. N. Borle, B. B. Sharma, R. K. Bagai and A. R. Kulkarni for their help and cooperation, Mrs. Geeta Mohan and Mrs Anita Sharma for technical support, and the Director, Solid State Physics Laboratory, for his permission to publish this work.

References

1. A. LASTRAS-MARTINEZ, V. LEE, J. ZEHNDER and P. M. RACCAH, *J. Vac. Sci. Technol.* **21** (1982) 157.
2. D. R. RHIGER and R. E. KVAAS, *ibid.* **21** (1982) 168.
3. M. SAKASHITA, H. H. STREHBLOW and M. BETTINI, *J. Electrochem. Soc.* **129** (1982) 1710.
4. H. J. RICHTER, U. SOLZBACH, M. SEELMANN-EGGEBERT, H. BRENDECKE, H. MAIER, J. ZIEGLER and R. KRUGER, in "Insulating Films on Semiconductors", Springer Series in Electrophysics, Vol. 7, edited by W. Engl (Springer-Verlag, Berlin, Heidelberg, New York, 1981) p. 298.
5. P. MORGEN, J. A. SILBERMAN, I. LINDAU, W. E. SPICER and J. A. WILSON, *J. Electron. Mater.* **11** (1982) 597.
6. T. S. SUN, S. P. BUCHNER and N. E. BYER, *J. Vac. Sci. Technol.* **17** (1980) 1067.
7. G. D. DAVIS, T. S. SUN, S. P. BUCHNER and N. E. BYER, *Proc. SPIE Infrared Detector Mater.* **285** (1981) 126.
8. J. S. AHEARN, G. D. DAVIS and N. E. BYER, *J. Vac. Sci. Technol.* **20** (1982) 756.
9. B. K. JANOUSEK and R. C. CARSCALLEN, *J. Appl. Phys.* **53** (1982) 1720.
10. R. L. STRONG, *J. Vac. Sci. Technol.* **5** (1987) 2003.
11. R. F. C. FARROW, P. N. J. DENNIS, H. E. BISHOP, N. R. SMART and J. T. M. WOTHERSPOON, *Thin Solid Films* **88** (1982) 87.
12. M. SEELMANN-EGGEBERT, G. BRANDT and H. J. RICHTER, *J. Vac. Sci. Technol.* **2** (1984) 11.
13. C. M. STAHLE, D. J. THOMSON, C. R. HELMS, C. H. BECKER and A. SIMMONS, *Appl. Phys. Lett.* **47** (1985) 521.
14. R. L. STRONG, J. M. ANTHONY, B. E. GNADE, J. A. KEENAN, E. NORBECK, L. W. LI and C. R. HELMS, *J. Vac. Sci. Technol.* **A4** (1986) 1992.
15. R. D. S. YADAVA, S. SINHA, B. B. SHARMA and A. V. R. WARRIER, *J. Crystal Growth* **73** (1985) 343.
16. R. D. S. YADAVA and A. V. R. WARRIER, *J. Electron. Mater.* **18** (1989) 537.
17. B. B. SHARMA and R. D. S. YADAVA, Technical Report. SPL 83 U1 (1983).
18. R. T. SANDERSON, "Chemical Bonds and Bond Energy" (Academic, New York, London, 1971) p. 57.
19. J. C. PHILLIPS, "Bonds and Bands in Semiconductors" (Academic, New York, 1973) Ch. 2.
20. T. C. HARMAN, in "Physics and Chemistry of II–VI Compounds", edited by M. Aven and J. S. Prener (North Holland, Amsterdam, 1967) p. 771.
21. W. ALBERS, *ibid.*, p. 209.
22. H. MAIER and J. HESSE, in "Crystals", edited by H. Freyhardt (Springer-Verlag, New York, 1977) p. 165.

Received 7 July
and accepted 12 December 1989